

Bayesian and Multi-Objective Decision Support for Real-Time Incident Mitigation in Critical Infrastructure

Shaofei Huang, Christopher M. Poskitt, Lwin Khin Shar

Singapore Management University, Singapore

Abstract

Critical infrastructure increasingly relies on interconnected cyber-physical systems whose security incidents can escalate rapidly into safety and operational failures. Existing decision-support approaches struggle to support real-time incident response because they rely on static assumptions, incomplete vulnerability data, and single-objective risk models that do not adequately capture trade-offs between attack likelihood, impact severity, and system availability. This paper proposes a real-time, adaptive decision-support framework for incident mitigation in critical infrastructure that combines hierarchical system modelling with Bayesian probabilistic reasoning. The framework leverages probabilistic graphical models (Bayesian Networks) constructed from system architecture and vulnerability data, and employs confidence-calibrated exposure estimation to integrate complementary vulnerability scoring metrics under epistemic uncertainty. Mitigation strategies are explored as countermeasure portfolios and refined using multi-objective optimisation to identify Pareto-optimal trade-offs suitable for time- and resource-constrained response scenarios. Frequency-based heuristics are applied to prioritise robust mitigation actions across optimisation runs. The framework is evaluated on three representative cyber-physical attack scenarios, demonstrating its ability to adapt to evolving threats and provide actionable decision support under real-time constraints, thereby enhancing the operational resilience of critical infrastructure.

Keywords: critical infrastructure, cyber-physical systems, incident response, decision-support systems, multi-objective optimisation, Bayesian Networks

1. Introduction

Cyber-Physical Systems (CPSs) form the backbone of modern critical infrastructure (CI), integrating digital and physical components to deliver the essential services that underpin modern society. While traditionally confined to centralised Industrial Control Systems (ICSs), CPSs are now deployed at scale across decentralised CI networks such as railway signalling networks and renewable energy ecosystems. This expansion has significantly broadened the attack surface for both state-sponsored and opportunistic actors, as digital vulnerabilities now translate directly into physical hazards and operational disruptions that threaten national security and public safety.

A pivotal example of this shifting threat landscape was highlighted in 2025 by the SUN:DOWN research report [11], which disclosed 46 new vulnerabilities across leading solar photovoltaic (PV) inverter vendors. These flaws, ranging from insecure cloud APIs to remote code execution, exposed severe systemic weaknesses in the renewable energy sector. Researchers demonstrated that by chaining these vulnerabilities, an adversary could orchestrate a coordinated load-changing attack, manipulating inverter output to destabilise grid frequency. Such an exploit could necessitate large-scale load shedding or trigger emergency equipment shutdowns, underscoring the existential risk that unsecured CPS components pose to infrastructural resilience.

Given the critical nature of these processes, *real-time* and *adaptive* decision support is essential to ensure robust security and incident mitigation, while simultaneously minimising impacts on safety and preserving continuous system availability. In this context, “real-time” refers to the decision-support window within which the CI operator needs to respond to preserve system stability, often under stringent latency constraints. “Adaptive” refers to the capacity to dynamically adjust mitigation strategies based on evolving threat conditions, system states, and resource availability. Unlike traditional IT environments, where remediation typically involves rapid software patching, CPS security decisions must balance cybersecurity objectives against physical process constraints [40]. In legacy CI, applying an unvalidated patch entails substantial operational risk. Updates may induce latent system failures or performance degradation, necessitating countermeasures that prioritise the resilience of CI systems [35].

Despite advancements in model-driven decision support, existing frameworks often operate under static assumptions and lack the adaptability required during an unfolding incident [29, 47]. Most frameworks cannot update model parameters such as vulnerability exposure probabilities or asset interdependencies in real

time. A representative scenario is the detection of a compromised communication dongle mid-response in a power grid. The inability to dynamically revise model attributes constrains operational decision-making and reduces response efficacy in time-critical contexts.

To address these limitations, we propose a real-time, adaptive decision-support framework for incident mitigation in critical infrastructure, grounded in applied probabilistic reasoning and designed to meet the operational realities of CI protection. We posit that effective response strategies must be guided by data-driven risk metrics while remaining bounded by stringent time and resource constraints. As illustrated in Figure 1, the proposed framework integrates Bayesian Network (BN) models for dynamic risk management [34, 48] with threat modelling informed by Failure Modes, Effects, and Criticality Analysis (FMECA) [3]. The key novelty lies in the operationalisation of confidence-calibrated exposure metrics, which bridge the gap between theoretical risk modelling and the practical demands of real-world CI incident response.

Contributions. The main contributions of our paper are summarised below:

- We present a Bayesian Network modelling approach designed explicitly for real-time, adaptive incident response in CI, rather than offline risk analysis. The model embeds system and vulnerability metadata in a Domain-Specific Language (DSL) [17], enabling rapid updates to structure and parameters as incidents unfold.
- We develop a hybrid exposure probability estimation framework that integrates complementary vulnerability scoring metrics through a Bayesian confidence calibration technique. This provides robust recommendations even under epistemic uncertainty stemming from incomplete or heterogeneous vulnerability metadata.
- We introduce a multi-objective decision-support methodology for incident mitigation in cyber-physical systems that balances security, safety, and operational resilience. By treating mitigation probabilities as dynamic decision variables, the framework identifies Pareto-optimal *countermeasure portfolios* tailored to CI constraints, and uses frequency-based heuristics to prioritise robust mitigation strategies under time- and resource-critical conditions.
- We demonstrate the applicability of the proposed framework through three representative CI case studies: the 2015 Ukrainian power grid (BlackEnergy) attack, a solar PV inverter system, and a railway CBTC network, demonstrating its effectiveness across diverse CI domains.

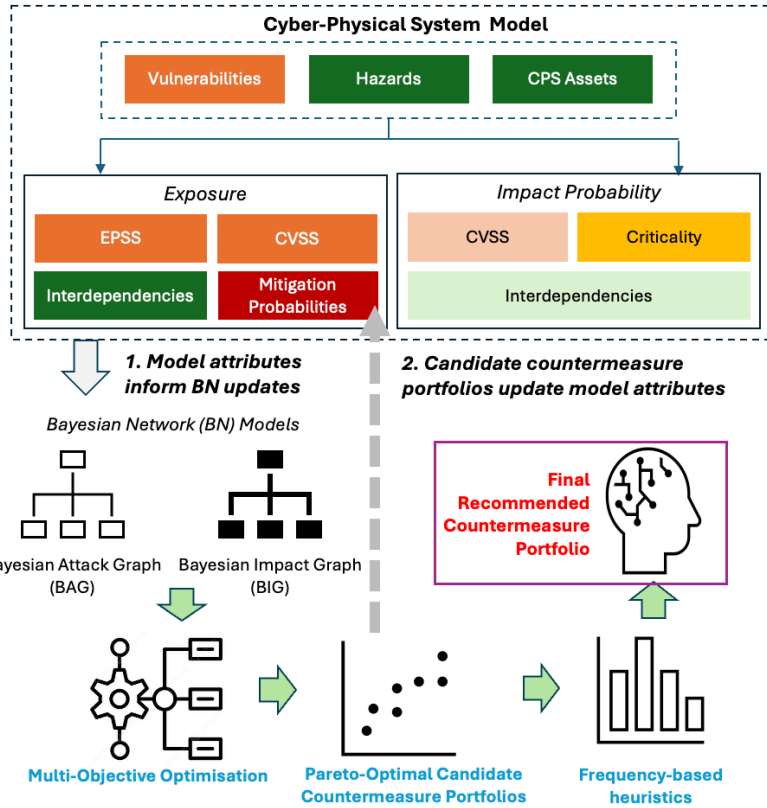


Figure 1: Architecture of our proposed critical infrastructure security framework. The diagram shows an iterative process integrating a CPS model (vulnerabilities, hazards, assets, exposure/impact probability attributes) with BN construction (BAG and BIG). Multi-objective optimisation generates Pareto-optimal countermeasure portfolios, updating model attributes and propagating exposure/impact probabilities. Frequency heuristic analysis selects the optimal portfolio.

- The models and source code developed in this research, along with the reference data and formulae used in the framework, are publicly available via the project’s GitHub repository [18]. This supports transparency, facilitates reproducibility and enables further development by both the research and practitioner communities within the CI protection domain.

The remainder of this paper is structured as follows. Section 2 provides background on the key techniques adopted in this work. Section 3 outlines the proposed methodology, including its theoretical foundations and implementation workflow, illustrated with a running example. Section 4 presents further applications of the framework to CI attack scenarios, accompanied by an analysis of

experimental results. Section 5 provides an in-depth, technical discussion of the findings and outlines directions for future research. Section 6 reviews related research and identifies limitations in existing approaches. Finally, Section 7 summarises the key contributions of the study.

2. Background

This section outlines the foundational techniques that underpin our proposed framework, including Bayesian networks, vulnerability scoring systems, and multi-objective optimisation.

Bayesian Networks. BNs are probabilistic graphical models that represent dependencies among variables using directed acyclic graphs, as illustrated in Figure 2. In cybersecurity, BNs are widely used to model attack propagation and risk inference [24], and also to support decision-making [22]. Specific to CPS, the works by Bhosale et al. [5, 6] discuss the adaptation of BN models to model probabilistic interdependencies between node types associated with CPS, namely, vulnerability nodes, which represent exploitable weaknesses in systems; asset nodes, which denote critical components within the CPS; and hazard nodes, which correspond to severe adverse outcomes including component failures.

Each node is associated with *exposure* and *impact* probability attributes that quantify the likelihoods of exploitation, failure dependencies, and cascading risks. These attributes shape the propagation of vulnerabilities and attack vectors, influencing the probabilities of attack success and of severe impact to the CI. Our work builds on these foundations by integrating such BN-based exposure and impact modelling into a real-time decision-support loop for incident mitigation, and by coupling the BN with optimisation and heuristic prioritisation to drive operational countermeasure selection rather than using the BN solely for static risk analysis.

Vulnerability Scoring Systems. The Common Vulnerability Scoring System (CVSS) provides a standardised framework for assessing the technical severity of vulnerabilities, with version 3.1 defining metrics to quantify exploitability and impact characteristics [16, 30]. However, as a deterministic scoring system, CVSS often fails to account for the inherent uncertainty and temporal dynamics of real-world attacks. The Exploit Prediction Scoring System (EPSS) addresses this limitation by providing probabilistic estimates of exploitation likelihood over the subsequent 30-day window, grounded in empirical indicators such as exploit availability and active exploitation trends [21].

To achieve a more granular assessment, our framework further integrates the *Known Exploited Vulnerabilities* (KEV) catalogue [9], which identifies vulnerabilities confirmed to have been exploited in real-world scenarios, alongside *Likely Exploited Vulnerabilities* (LEV) [31] data, which provides daily probability estimates of observed exploitation activities. By incorporating both authoritative records and statistical exploitation estimates, our approach captures a broader spectrum of the threat landscape.

Our framework distinguishes itself by fusing these complementary scoring schemes within a Bayesian calibration mechanism, yielding uncertainty-aware exposure probabilities that explicitly account for incomplete or heterogeneous vulnerability metadata, and by embedding these calibrated probabilities directly into the BN that underpins our decision-support process.

Multi-Objective Optimisation. CI decision makers are often constrained by fixed budgets that fall short of the minimum cost required for comprehensive system hardening. The challenge lies in selecting a subset of security measures that remain within budget while minimising residual risk from unaddressed vulnerabilities [13]. Multi-objective optimisation addresses this challenge by identifying solutions that balance competing objectives, such as cost, system availability, and risk reduction. Prior research has explored Bayesian optimisation and evolutionary strategies to derive optimal security configurations under uncertainty and resource constraints [13, 29]. In particular, the work by Zebrowski et al. [48] formulates the optimisation task as a Pareto-efficient portfolio selection problem, leveraging a Bayesian Network to identify security measures that simultaneously minimise various types of expected cyberattack impacts, while satisfying budgetary and other constraints. While this approach is highly applicable to CI environments, our work extends it by treating mitigation probabilities as parameters that shape the decision variables within the optimisation space, repeatedly updating BN parameters in response to candidate portfolios, and applying frequency-based heuristic analysis across multiple optimisation runs to prioritise countermeasures under time- and resource-constrained, real-time incident response conditions.

3. Methodology

This section describes the methodology of our proposed framework, illustrated with a running example of a solar PV inverter attack, which is based on the security reports by Dabrowski et al. [10] and Dashevskyi et al. [11]. In particular, we refer to their identified CVE (Common Vulnerabilities and Exposures) entries

that can be chained to form hypothetical attack paths targeting solar PV inverter systems. While Dabrowski et al. originally proposed destabilising the power grid via coordinated load modulation from a botnet of consumer devices, our scenario explores a complementary threat vector focused on the supply side. Here, the adversary leverages mobile or web applications to obtain sensitive information, which is then used to compromise a message broker and subsequently a controller linked to both the message broker and a solar PV inverter. Once initial access is established, the attacker hijacks additional inverters and synchronises their configuration changes to create abrupt fluctuations in grid input. By overwhelming the grid's balancing mechanisms, this coordinated attack can degrade grid stability or induce power outages, thereby achieving the attacker's ultimate objective.

Overview. Our framework (Figure 1) begins with the construction of a BN model that defines a shared structure for attack and impact graphs, informed by CPS system attributes and the attack scenario. Randomised mitigation probability values are introduced as initial inputs into a multi-objective optimisation process, which generates candidate countermeasure portfolios aimed at maximising system availability while minimising the likelihood of attack success and severe impact occurrence. These portfolios are subsequently reintegrated into the BN as updated mitigation probabilities, and the optimisation cycle is repeated across multiple trials within a single run. The top-performing portfolios from these iterative runs are then analysed using frequency-based heuristics to identify vulnerability nodes within the attack path that consistently exhibit high mitigation effectiveness. This insight serves to guide final prioritisation decisions during incident response, particularly when confronted with stringent time and resource limitations. The high-level steps of our proposed framework are outlined in Algorithm 1. Each step is elaborated in detail in Sections 3.1 to 3.6.

3.1. Bayesian Network Model Construction

In the first step of our methodology, we construct an abstract BN model that captures the relevant cyber-physical structure of the target CPS and the incident under consideration. **Nodes** represent *CPS assets*, *vulnerabilities*, or *hazards*, while **directed edges** encode the causal and conditional dependencies through which attacks and failures may propagate. The model is instantiated using system-specific architectural information and operational knowledge, typically elicited from domain experts or system documentation, together with vulnerability data drawn from CVE repositories or expert judgement.

This BN serves as a shared structural backbone for both the *Bayesian Attack Graph (BAG)* and the *Bayesian Impact Graph (BIG)* used in subsequent stages

Algorithm 1 Methodology of Proposed CI Decision Support Framework

- 1: **Build** BN model integrating CPS metadata and attack scenario context, encoded in AutomationML (§ 3.1)
 - 2: **Compute** exposure probabilities for nodes within the BN model, representing likelihoods of attack success (§ 3.2)
 - 3: **Calculate** propagated impact probabilities resulting from exploitation or failure of BN nodes (§ 3.3)
 - 4: **Calculate** posterior likelihoods of successful attack and severe impact, conditioned on observed evidence within the BN model (§ 3.4)
 - 5: **for** num_runs = 1 to max_num_runs **do**
 - 6: **for** num_trials = 1 to max_num_trials **do**
 - 7: **Run** multi-objective optimisation to generate candidate countermeasure portfolios (§ 3.5)
 - 8: **Update** BN model mitigation attributes using top-performing candidate portfolio
 - 9: **end for**
 - 10: **Identify** high-impact mitigation nodes for prioritisation under time and resource constraints, by analysing frequency-based heuristics of top-performing portfolios (§ 3.6)
 - 11: **end for**
 - 12: **Recommend** final countermeasure portfolio
-

of the framework. Given the fixed structure, we incorporate scenario-specific assumptions and hypothesised attack paths to populate asset, vulnerability, and hazard nodes, and encode the resulting model in AutomationML (XML based data modeling language for representing engineering models) [14] to support systematic analysis and downstream optimisation.

Running Example. Figure 2 shows a Bayesian Network graph of a solar PV inverter attack scenario. The BN model was constructed by mapping system topology and functional interdependencies referenced from the work by Dashevskiy et al. [11]. CPS asset, vulnerability, and hazard nodes are instantiated using information from CVE repositories alongside the attack scenario [10].

3.2. Exposure Probability Calculations

This subsection outlines our methodology used to compute probabilities of attack success, which we term as *exposure*, for vulnerability, asset, and hazard nodes within the BN representation.

Vulnerability Nodes. The approach for vulnerability nodes needs to account for both publicly disclosed vulnerabilities with CVE identifiers, and proprietary or undocumented vulnerabilities lacking formal CVE enumeration. To calculate the

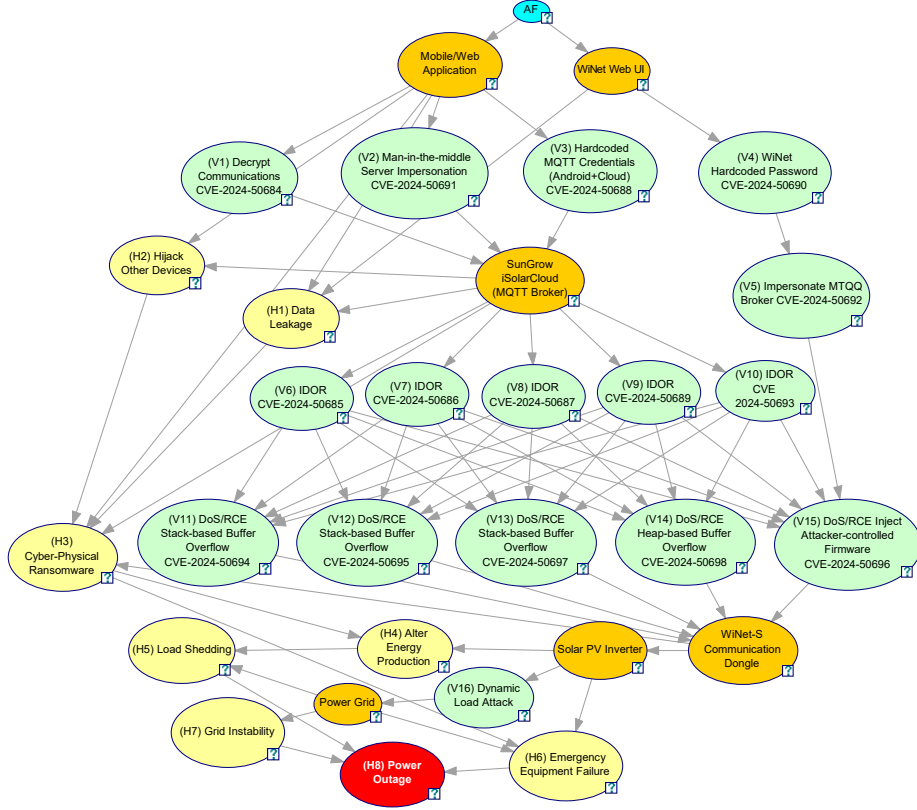


Figure 2: Bayesian Network of a hypothetical cyber-physical attack on solar PV inverters connected to a power grid. Node colours denote assets (orange), vulnerabilities (green), hazards (yellow), attack feasibility (cyan), and attacker goal (red). A high-resolution version of the graph is available in the project’s GitHub repository [18].

exposures of CVE-linked vulnerability nodes, we use EPSS, LEV, and KEV metrics in conjunction with the *maximal-envelope approach* introduced by Mell et al. [31] to select the highest exposure probability among these complementary vulnerability scoring frameworks.

The Likely Exploited Vulnerability (LEV) metric is defined by Mell et al. as:

$$\text{LEV}(v, d_0, d_n) \geq 1 - \prod_{\forall d_i \in \text{dates}(d_0, d_n, 30)} (1 - \text{epss}(v, d_i) \times \text{weight}(d_i, d_n, 30)) \quad (1)$$

where v is the vulnerability; d_0 is the first date on which an EPSS score is available; d_n is the date on which the calculation is performed (usually the present day);

$\text{epss}(v, d)$ is the EPSS score for vulnerability v on date d ; and $\text{weight}(d_i, d_n, w)$ is the number of days between d_i and d_n , limited by the window size w , divided by w .

The probability of exposure for a CVE-linked vulnerability, $P(E)_{\text{vuln, CVE}}$ is defined as:

$$P(E)_{\text{vuln, CVE}} = \max(\text{EPSS}, \text{LEV}, \text{KEV}) \quad (2)$$

where $\text{KEV} \in \{0, 1\}$ acts as a logical ceiling, ensuring that any vulnerability confirmed to have been exploited in real-world scenarios is assigned a maximal exposure probability of 1; otherwise, it is assigned 0. Notably, if $\text{KEV} = 1$, $P(E)_{\text{vuln, CVE}}$ becomes 1 regardless of EPSS or LEV, as this is a critical safety-conservative assumption for CI.

For proprietary or undocumented vulnerabilities lacking CVE identifiers, EPSS, LEV, and KEV metrics are unavailable for exposure probability calculation. Proxy CVSS scores are therefore derived from the exploitability subscore of the CVSS base metrics, computed as follows:

$$P(E)_{\text{vuln, non-CVE}} = AV \times AC \times PR \times UI \quad (3)$$

where AV , AC , PR , and UI represent the Attack Vector, Attack Complexity, Privileges Required, and User Interaction metrics, respectively. Each metric is assigned the corresponding numerical weight per the CVSS v3.1 specification [16].

As shown by Wunder et al. [43], epistemic uncertainty persists in CVSS evaluations [43]. To address this, we employ a *Bayesian confidence calibration technique* inspired by Küppers et al. [28]. We model the observed proxy CVSS score as a distribution linked to a shared latent variable $P(E)_{\text{vuln}}^*$, representing the unobserved true probability of exposure:

$$P(E)_{\text{vuln, non-CVE}} \sim \mathcal{N}(P(E)_{\text{vuln}}^*, \sigma_{\text{CVSS}}^2) \quad (4)$$

Assuming a Gaussian prior as in [25], where $P(E)_{\text{vuln}}^* \sim \mathcal{N}(\mu_0, \sigma_0^2)$, the Bayesian latent variable formulation for the posterior parameters is represented as:

$$\mu_{\text{post}} = \frac{\frac{\mu_0}{\sigma_0^2} + \frac{P(E)_{\text{vuln. CVSS}}}{\sigma_{\text{CVSS}}^2}}{\frac{1}{\sigma_0^2} + \frac{1}{\sigma_{\text{CVSS}}^2}} \quad (5)$$

$$\sigma_{\text{post}}^2 = \left(\frac{1}{\sigma_0^2} + \frac{1}{\sigma_{\text{CVSS}}^2} \right)^{-1} \quad (6)$$

The resulting calibrated exposure probability estimate $P(E)_{\text{vuln}}^* \sim \mathcal{N}(\mu_{\text{post}}, \sigma_{\text{post}}^2)$, serves as a unified, uncertainty-aware input for downstream attack propagation and mitigation optimisation within the BN graphs.

In addition, we incorporate an *Attack Feasibility* (AF) modifier, inspired by the work of Xie et al. [44], to ensure the formulation reflects real-world conditions more accurately. This modifier is applied to the probability calculations for all vulnerability nodes. Specifically, the AF modifier adjusts probability estimations by accounting for the system's security posture, adversary capabilities, and environmental constraints. For instance, systems featuring robust, up-to-date defences and restricted access protocols yield lower AF values, reflecting a reduced likelihood of exploitation. Conversely, an unpatched CPS targeted by a sophisticated adversary results in a higher probability of a successful attack. Consequently, the final probability of a successful attack for a given vulnerability node, irrespective of whether it has a CVE identifier, is defined as:

$$P(A)_{\text{vuln}} = P(E)_{\text{vuln}} \times \phi \quad (7)$$

where:

- $P(A)_{\text{vuln}}$ represents the probability that an attack of the vulnerability node is successful.
- $P(E)_{\text{vuln}}$ denotes the probability of exposure for the vulnerability.
- ϕ is the attack feasibility (AF) modifier, representing context-specific variables such as system defence posture, adversary capability, and environmental constraints.

Asset Nodes. For an *asset node*, the probability of exposure corresponds to the probability of asset failure and is calculated using an exponential decay function, which models failure likelihood over time:

$$P(E)_{\text{asset}} = 1 - e^{-\lambda t} \quad (8)$$

where λ represents the failure rate per unit time, determining how frequently the asset is expected to degrade, and t denotes the operational duration, reflecting the asset’s time in service.

This formulation is grounded in Markov-based reliability analysis [26], in which asset failures are modelled as a stochastic process, capturing the progressive deterioration of system components over time. By incorporating time-dependent degradation patterns, this approach provides a probabilistic estimation of failure likelihood, supporting predictive maintenance and risk-informed decision-making in CI environments.

Hazard Nodes. Finally, *hazard nodes* represent hazardous events, failures, or disruptions influenced by attack propagation. As such, the occurrence of a hazard is influenced by the cyber-physical dependencies within the system. If the parent node of a hazard is an asset, then the failure of that asset increases the likelihood of hazard activation. Similarly, if the parent node is another hazard, its occurrence propagates risk, potentially escalating the attack scenario.

To represent hazard occurrence probabilistically, the probability of exposure for a hazard node is defined as:

$$P(E)_{\text{haz}} = \begin{cases} 1, & \text{if parent asset fails or parent hazard occurs} \\ 0, & \text{otherwise} \end{cases} \quad (9)$$

This binary assignment ensures deterministic modelling of attack escalation and structured attack progression through hazard nodes, where asset failures or hazard dependencies directly influence security outcomes.

Running Example. In our running example of a solar PV inverter, EPSS scores and KEV catalog entries for CVE identifiers of vulnerability nodes are retrieved from the FIRST EPSS and CISA databases respectively. LEV scores are computed per Equation 1 using EPSS scores over a 30-day window ($w = 30$). For vulnerability node V8 (CVE-2024-50687: iSolarCloud API allows unauthorised access to Sungrow device data and parameters), these metrics are presented in Table 1. Equation 2 then yields a final exposure probability of $P(E)_{V8,CVE} = 0.0342$.

For the single vulnerability node V16, which does not have a CVE identifier and represents a dynamic load-changing attack on the power grid, we approximate the CVSS-proxy vector based on information from the literature [10].

CVSS:3.1/AV:N/AC:L/PR:N/UI:N/S:C/C:N/I:L/A:H

Table 1: Vulnerability metrics for CVE-2024-50687 (retrieved 2026-02-15). Despite a high CVSS score (9.1), the LEV-derived exposure probability remains low (0.0342), indicating that although the vulnerability has a high theoretical severity score, it is unlikely to be exploited in real-world scenarios.

Scoring System	Score
CVSS v3.1	9.1
EPSS (Latest Score)	0.0012
LEV	0.0342 (3.42%)
KEV	0 (Not listed in CISA catalogue)
$P(E)_{V8, CVE}$	0.0342

This CVSS vector characterises a network-accessible attack within the critical infrastructure: AV:N indicates remote exploitation over a network; AC:L denotes low complexity requiring no specialised preconditions; PR:N and UI:N show that no privileges or user interaction are needed; S:C reflects changed scope impacting beyond the target system; C:N indicates no confidentiality loss; I:L shows low integrity compromise; while A:H signifies high availability impact. Using Equation 3 with the corresponding CVSS metric values [16], the fallback exposure probability estimate for V16 is calculated as:

$$P(E)_{V16, non-CVE} = 0.85 \times 0.77 \times 0.85 \times 0.85 = 0.4729 \quad (10)$$

Next, we apply our Bayesian confidence calibration technique to the fallback exposure probability estimate $P(E)_{V16, non-CVE}$ to improve its realism and robustness. First, a standard deviation of 0.2 is assigned to reflect the low confidence level of the CVSS-proxy estimation, yielding a likelihood variance of $\sigma_{CVSS}^2 = 0.04$. For the prior distribution, a mean of $\mu_0 = 0.5$ and a variance of $\sigma_0^2 = 0.0025$ (corresponding to a standard deviation of 0.05) are assigned to reflect a neutral initial belief in the distribution. Substituting these values into Equations 5 and 6 yields the following:

$$\mu_{\text{post}} = \frac{(0.5/0.0025) + (0.4729/0.04)}{(1/0.0025) + (1/0.04)} = \frac{200 + 11.8225}{400 + 25} \approx \mathbf{0.4984} \quad (11)$$

$$\sigma_{\text{post}}^2 = \left(\frac{1}{0.0025} + \frac{1}{0.04} \right)^{-1} = (400 + 25)^{-1} = \mathbf{0.00235} \quad (12)$$

The low posterior variance of $\sigma_{\text{post}}^2 = 0.00235$ indicates that the calibrated,

posterior vulnerability exposure probability estimate of $\mu_{\text{post}} \approx 0.4984$ can be used with relatively high confidence.

Additionally, an AF modifier of $\phi = 1.0$ is applied to all vulnerability node exposure probabilities using Equation 7 to reflect an idealised modelling assumption in which the adversary possesses unrestricted access and capability, and the target system exhibits minimal defensive barriers.

To calculate asset node exposure probabilities using Equation 8, the operational duration of all assets is defined from 1 January 2024 to the current date, for simplicity. Failure rates for assets, such as the WiNet-S communication dongle connected to the inverter, are estimated based on published literature [5] and technical specifications of comparable components available online. Finally, Equation 9 is used to assign exposure probabilities to the corresponding hazard nodes within the BN graph.

3.3. Impact Probability Calculations

This subsection outlines our methodology for computing the propagated impact probabilities arising from exploitation or failure of vulnerability, asset, and hazards nodes within the BN graph.

Vulnerability Nodes. In the case of vulnerability nodes (both CVE- and non-CVE-linked), we use the following formulation, drawing on the corresponding CVSS metric values [16], to compute the probability of impact:

$$P(\text{Impact})_{\text{vuln}} = 1 - [(1 - C) \cdot (1 - I) \cdot (1 - A)] \quad (13)$$

where:

- $P(\text{Impact})_{\text{vuln}}$ denotes the probability of severe impact associated with the vulnerability node.
- C, I, A represent the confidentiality, integrity, and availability impact metrics, respectively. For vulnerabilities that do not have CVE identifiers, the impact metrics are estimated based on available system context, attack surface semantics, or analogous vulnerabilities with similar functionality.

Asset and Hazard Nodes. In the case of asset and hazard nodes, the probability of impact is determined by the number of child nodes each individual node directly influences, reflecting its potential to propagate disruption or failure through the system [2, 5]. This is formulated as:

$$P(\text{Impact})_{\text{asset, haz}} = \frac{\text{Number of connected child nodes}}{\text{Total number of nodes in the BN graph}} \quad (14)$$

This normalised formulation ensures that the impact probability lies within the interval $[0, 1]$, and that asset or hazard nodes with higher structural influence, through greater downstream reach, are assigned proportionally higher impacts.

Running Example. In our running example, the impact probabilities of vulnerability nodes are calculated using Equation 13, drawing on the confidentiality, integrity, and availability metric values derived from their respective CVSS vectors. For instance, the vulnerability node V8 (CVE-2024-50687) has a CVSS vector: CVSS:3.1/AV:N/AC:L/PR:N/UI:N/S:U/C:H/I:H/A:N. Here, C:H indicates high confidentiality loss (metric value: 0.56); I:H shows high integrity compromise (metric value: 0.56); and A:N signifies no availability impact (metric value: 0). Accordingly, the impact probability for this vulnerability node is calculated as follows:

$$P(\text{Impact})_{V8} = 1 - [(1 - 0.56) \times (1 - 0.56) \times (1 - 0)] = 0.8064 \quad (15)$$

Within the solar PV inverter BN presented in Figure 2, which comprises 30 nodes in total, the impact probabilities of hazard and asset nodes are derived from the underlying interdependencies among them. For illustration, successful exploitation of an asset node *app*, specifically the Sungrow iSolarCloud mobile/web application, directly influences three vulnerability nodes: V1, V2, and V3. Using Equation 14, this asset node’s impact probability is calculated as follows:

$$P(\text{Impact})_{app} = \frac{3}{30} = 0.1 \quad (16)$$

3.4. Posterior Probability Calculations

Once the exposure and impact probabilities for vulnerability, asset and hazard nodes are calculated, the posterior likelihood of successful attack and the probability of severe impact to the CPS, given the evidence of a vulnerability node being exploited, for example, can be derived using conditional probability tables and variable elimination [49].

Running Example. For the running example, the joint conditional probabilities for exposure and impact associated with the attacker’s goal: H8_Power_Outage

Table 2: Joint Conditional Probability Table for Exposure and Impact of H8_Power_Outage

State	$\phi_{\text{Exposure}}(\text{H8_Power_Outage})$	$\phi_{\text{Impact}}(\text{H8_Power_Outage})$
(0)	0.2555	0.9153
(1)	0.7445	0.0847

are shown in Table 2. These values are derived from Bayesian inference computations based on estimates, posterior parameters and updated evidence from the risk model.

The results indicate that the posterior likelihood of a successful attack (exposure) is $P(E) = 0.2555$, while the posterior probability of severe impact on the CI is $P(I) = 0.9153$. Multiplying these yields a composite risk score of $R = P(E) \times P(I) = 23.39\%$, highlighting the potential for high-impact outcomes even when the estimated probability of attack success is relatively moderate.

3.5. Multi-Objective Optimisation

Our framework employs multi-objective optimisation to assess and weigh trade-offs between *countermeasure portfolios*, *failure probabilities* and *impact ratings* to inform consequence-driven and risk-informed decision support in CPS.

Countermeasure Portfolios. Countermeasure portfolios are instantiated as tuples of *Probability of Mitigation* attributes, embedded within each vulnerability node in the BAG and BIG models. Each portfolio is defined as an ordered tuple

$$\mathbf{M} = (P(M_1), P(M_2), \dots, P(M_n))$$

comprising the mitigation probabilities $P(M_i)$ associated with each vulnerability V_i ($i = 1, 2, \dots, n$) in the BAG model. A higher mitigation probability implies a lower likelihood of successful exploitation at the corresponding node. The ordering of nodes within these tuples reflects the relative effectiveness of mitigation strategies, thereby guiding prioritisation under resource and time constraints.

Failure Probabilities. The first author’s professional experience suggests that asset failure probabilities can be influenced by mitigation-induced risks. For instance, the application of faulty or unstable security patches to a CPS asset may introduce unintended consequences, including asset failure. This complexity is exacerbated when an asset is linked to multiple vulnerabilities, each associated with distinct mitigation-related risks. In our framework, each countermeasure

is associated with a risk adjustment function that governs its net contribution to asset-level failure. Accordingly, the failure probability of a CPS asset is defined as a bounded, risk-adjusted function of the mitigations applied across its associated vulnerabilities:

$$P(F_a | \mathbf{M}) = \min \left(1.0, \kappa_a \cdot \sum_{i \in \mathcal{V}_a} P(\text{Fail}_{\text{mit}}^i) \right) \quad (17)$$

where:

- $P(F_a | \mathbf{M})$ is the probability of failure for CPS asset a given the countermeasure portfolio \mathbf{M} ;
- \mathcal{V}_a is the set of vulnerabilities associated with asset a ;
- $P(\text{Fail}_{\text{mit}}^i)$ is the probability that mitigation applied to vulnerability i causes unintended adverse consequences that contribute to asset failure;
- $\kappa_a \in (0, 1]$ is a scaling constant ensuring proportionality and bounding;
- The min function ensures the total failure probability remains within the interval $[0, 1]$.

This formulation enables our framework to support dynamic risk assessments in scenarios where mitigation strategies evolve over time or new vulnerabilities are discovered.

Impact Ratings. Another important element in the framework is the *Impact Rating* attribute, embedded in asset and hazard nodes. This rating captures the multifaceted consequences of successful attacks across safety, operational, financial and informational domains. It is computed by adapting the formulation proposed by Amro et al. [3]:

$$\text{Impact Rating} = \sum_{j \in \{S, F, I, O, C\}} (\text{Factor}_j \cdot \text{Criticality}_j) \quad (18)$$

where:

- S: safety impact — refers to potential harm to human life or physical injury resulting from a CPS failure or security breach.
- F: financial impact — quantifies monetary losses due to CPS equipment damage, service downtime or disrupted business operations.

- I: informational impact — relates to the compromise, loss or exposure of sensitive data and system configurations.
- O: operational impact — reflects the degree to which core CPS functions or processes are degraded or interrupted.
- C: staging impact — indicates the ability to enable further attacks or facilitate persistence, privilege escalation or lateral movement.
- Factor_{*j*}: the relative weight assigned to impact type *j*.
- Criticality_{*j*}: the criticality level associated with impact type *j*.

The optimisation process begins by randomly generating countermeasure portfolios, denoted as

$$\mathbf{M}^{(j)} \quad (j = 1, 2, \dots, n)$$

Each portfolio's mitigation values are encoded into the BN model and used to infer the posterior probabilities of both attack success and severe impact on the CI, via Bayesian inference algorithms. These probabilistic outcomes are treated as parameters within a multi-objective search space. Pareto-optimal portfolios are then identified using the Optuna library [1], balancing the competing objectives of minimising the likelihood of attack success, and at the same time, minimising the probability of severe impact and maximising system availability. The resulting Pareto fronts form the foundation of our proposed decision support mechanism.

Running Example. In our running example, Equation 17 is used to calculate the risk-adjusted failure probabilities of CPS assets such as the WiNet-S communication dongle, which are connected to multiple vulnerability nodes, each associated with distinct mitigation-related risks.

Equation 18 is used to calculate impact ratings. As shown in Table 3, the impact rating of the solar PV inverter is calculated to be 0.3864. This figure arises from assigning a maximum safety factor of 1.0, based on the overarching principle that safety must never be compromised, although the associated criticality is 0, as no injuries are anticipated in the event of failure. Financial impact carries a weight of 0.25 and a criticality of 0.25, signifying localised equipment damage. The informational dimension, also weighted at 0.25, presents a higher criticality of 0.75 owing to the component's role in managing system configurations that could substantially affect overall CPS security. Operationally, the component is heavily weighted (0.75) with a matching criticality of 0.75, as it directly influences CI operations – its failure potentially leading to cascading outages or grid instability.

Table 3: Impact Ratings for Solar PV Inverter Components

Component	F_S	S	F_F	F	F_I	I	F_O	O	F_C	C	Impact Rating
Mobile/Web App	1	0	0.25	0	0.25	0.5	0.75	0	0.5	0.25	0.0909
WiNet Web	1	0	0.25	0	0.25	0.5	0.75	0	0.5	0.25	0.0909
MQTT Broker	1	0	0.25	0	0.25	0.5	0.75	0.5	0.5	0.5	0.2727
WiNet-S Dongle	1	0	0.25	0	0.25	0.5	0.75	0.5	0.5	0.5	0.2727
PV Inverter	1	0	0.25	0.25	0.25	0.75	0.75	0.75	0.5	0.5	0.3864
Power Grid	1	0.5	0.25	0.75	0.25	0	0.75	1	0.5	0.75	0.6591

Finally, the staging impact holds a moderate weight of 0.5 and a criticality of 0.5, denoting the component’s potential to facilitate attacker persistence or lateral movement.

Finally, a multi-optimisation study is performed to identify Pareto-optimal countermeasure portfolios. The scatter plot (Figure 3) reveals a consistent curved slope across the likelihood and impact axes, with data points forming a relatively smooth trajectory that appears to ascend with increasing impact levels. This suggests a stable correlation between these dimensions, wherein higher-impact and higher-availability scenarios tend to co-occur. The continuity of the slope implies underlying systemic regularities, potentially driven by latent causal BN-represented structures within the CI environment. The scatter plot also displays a plateau between approximately 0.25 and 0.30 along the *Impact* axis. This observation indicates that a subset of countermeasure portfolios successfully reduce the likelihood of severe impact, yet offer limited gains in system availability.

3.6. Frequency-Based Heuristic Analysis

Lastly, a frequency-based heuristic analysis of Pareto-optimal portfolios is conducted across multiple optimisation runs to rank and identify the vulnerability nodes that most consistently and effectively contributed to high-performing countermeasure configurations. These nodes are strong candidates for prioritisation in mitigation strategies, particularly under time and resource constraints during incident response.

Running Example. As shown in Figure 4, vulnerabilities V1 through V4 demonstrate consistently high mitigation effectiveness across numerous portfolio instances. This finding is corroborated by the underlying Bayesian Network structure (Figure 2), which reveals that these vulnerabilities constitute critical entry points, facilitating downstream attack propagation throughout the CI.

In summary, the key findings of the running example of a solar PV inverter attack are:

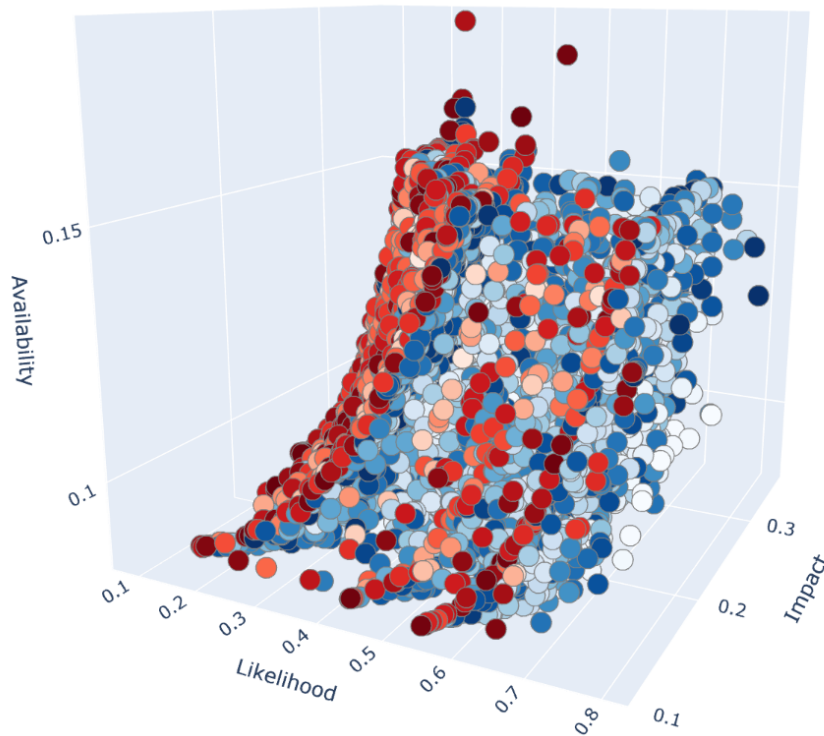


Figure 3: Pareto fronts derived over 10,000 multi-objective optimisation trials in the solar PV inverter case study

- Optimisation results reveal systemic regularity, suggesting latent causal structures within the BN structure.
- A subset of countermeasure portfolios successfully reduce the likelihood of severe impact, yet offer limited gains in system availability.
- Vulnerabilities V1–V4 demonstrated consistently high mitigation effectiveness, reflecting their positions as critical entry points in the BN structure.

Taken together, these findings point to several practical implications for CI practitioners. The observed systemic regularity invites further investigation into causal structures, potentially enabling more targeted interventions. Furthermore, the limited availability gains observed suggest the need for integrating complementary strategies such as anomaly detection, automated containment, or real-time system reconfiguration to strengthen operational resilience. The consistent

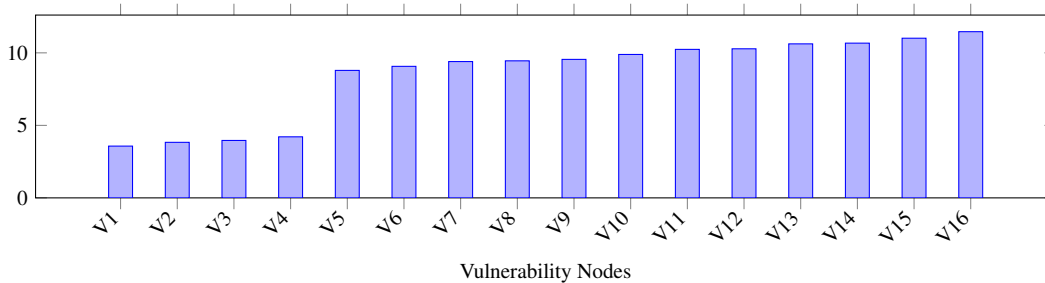


Figure 4: Average rank positions of mitigation probabilities across 100 runs of 10,000 optimisation trials in each run

effectiveness of vulnerabilities V1–V4 reinforces their prioritisation as part of any initial mitigation sweep, especially in scenarios involving time- and resource-constrained decision-making.

4. Further Evaluation Across CI Scenarios

This section evaluates the practical utility and applicability of our proposed framework by applying the methodology to another two representative CI scenarios beyond the initial solar PV inverter case study. The corresponding results are presented and analysed to highlight key insights, limitations, and implications for real-world deployment.

4.1. Ukrainian Power Grid (BlackEnergy) Attack

Our proposed framework is applied to enable real-time, adaptive mitigation of the 2015 Ukrainian power grid attack, which notoriously leveraged the BlackEnergy malware to attack a CPS [36]. Figure 5 presents the corresponding Bayesian Network graph of the attack tree [27] created with the GeNIe Academic tool [12]. Based on this structure, the BN model is constructed using available information to define the asset, vulnerability, and hazard nodes, and encoded in AutomationML [4].

Next, we calculate the exposure and impact probability values using the methodology outlined in Section 3. Two of the vulnerability nodes are listed in the National Vulnerability Database (NVD) [32] with CVE identifiers; the rest are not. Table 4 presents the vulnerability metrics for vulnerability node V2 (CVE-2014-1761: Microsoft Word Remote Code Execution). Equation 2 yields a final maximum exposure probability of $P(E)_{V2,CVE} = 1.0$.

Table 4: Vulnerability metrics for CVE-2014-1761 (retrieved 2026-02-15). Despite age (>10 years), high CVSS (7.8), LEV (1.0), and KEV listing yield maximum exposure probability (1.0) – indicating the vulnerability is almost certain to be exploited in real-world scenarios.

Scoring System	Score
CVSS v3.1	7.8
EPSS (Latest Score)	0.9313
LEV	1.000 (100%)
KEV	1 (Listed in CISA catalogue)
$P(E)_{V3, CVE}$	1.0

control, and potential operational failure. Based on the CVSS vector, the fallback exposure probability estimate is derived as:

$$P(E)_{V3, non-CVE} = 0.306 \quad (19)$$

We further calibrate this estimate using Equation 5, arriving at a corresponding likelihood variance of $\sigma_{CVSS}^2 = 0.04$ based on a standard deviation of 0.2. The low variance reflects low confidence in a heuristic-based exposure probability estimate. Additionally, the prior distribution assumes a mean of $\mu_0 = 0.5$, representing a midpoint assumption about exploitability in the absence of external evidence, and a variance of $\sigma_0^2 = 0.0025$ based on a standard deviation of 0.05, reflecting high confidence in this prior belief. Using the Bayesian latent variable formulation (cf. Equation 5), the posterior distribution is thus:

$$\mu_{\text{post}} = \frac{(0.5/0.0025) + (0.306/0.04)}{(1/0.0025) + (1/0.04)} = \frac{207.65}{425} \approx \mathbf{0.489} \quad (20)$$

$$\sigma_{\text{post}}^2 = \left(\frac{1}{0.0025} + \frac{1}{0.04} \right)^{-1} = (400 + 25)^{-1} = \mathbf{0.00235} \quad (21)$$

This yields a calibrated exposure probability estimate of approximately 0.489 with a posterior variance of 0.00235. The low posterior variance indicates that the posterior estimate can be used with relatively high confidence within the Bayesian network. Using this procedure, the calibrated exposure probability estimates for all vulnerabilities in the BlackEnergy attack model are computed.

Table 5 presents the conditional probabilities for exposure and impact associated with the attacker’s goal: H5.Disable.Electrical.Supply, derived using

Table 5: Joint Conditional Probability Table for Exposure and Impact of H5_Disable_Electrical_Supply

State	$\phi_{\text{Exposure}}(\text{Goal})$	$\phi_{\text{Impact}}(\text{Goal})$
(0)	0.8750	0.2393
(1)	0.1250	0.7607

Bayesian inference via variable elimination. The results show a posterior likelihood of successful attack of $P(E) = 0.8750$ (using an AF modifier of $\phi = 1.0$), and a corresponding posterior probability of severe impact on the CPS of $P(I) = 0.2393$. The composite risk score is computed as $R = P(E) \times P(I) = 20.94\%$ in the BlackEnergy attack.

Table 6: Top-performing countermeasure portfolio from the BlackEnergy case study. The countermeasure portfolio was optimised to minimise the likelihood of attack success and severe impact, while maximising CPS availability.

Metric	Value
Trial ID	9683
Countermeasure portfolio	V1:0.9901, V2:0.9855, V3:0.9777, V4:0.9821, V5:0.9954, V6:0.9892, V7:0.9824, V8:0.9903, V9:0.9713, V10:0.9722, V11:0.9772
Likelihood of successful attack	0.1486
Probability of severe impact	0.2899
Availability	0.6766

Next, we performed optimisation studies to search for Pareto-optimal countermeasure portfolios to support decision-making in mitigating the BlackEnergy attack. Figure 6 reveals an increasingly linear relationship between impact probability and system availability at higher impact probability levels. Additionally, the Pareto fronts appear clustered near a similar value along the attack likelihood axis, suggesting limited variation in attack likelihood across trials.

Analysis of the top-performing countermeasure portfolio presented in Table 6 highlights a clear trade-off between exposure, impact, and system availability. The model prescribes near maximal intervention across all identified vulnerabilities, with mitigation parameters approaching unity. Despite these intensive efforts, the probability of severe impact remains moderate. This suggests that in the context of the BlackEnergy attack, aggressive mitigation successfully bolsters system availability but fails to fully suppress the residual risk of severe impact on the CPS. Such a result indicates that structural interdependencies within CIs may sustain

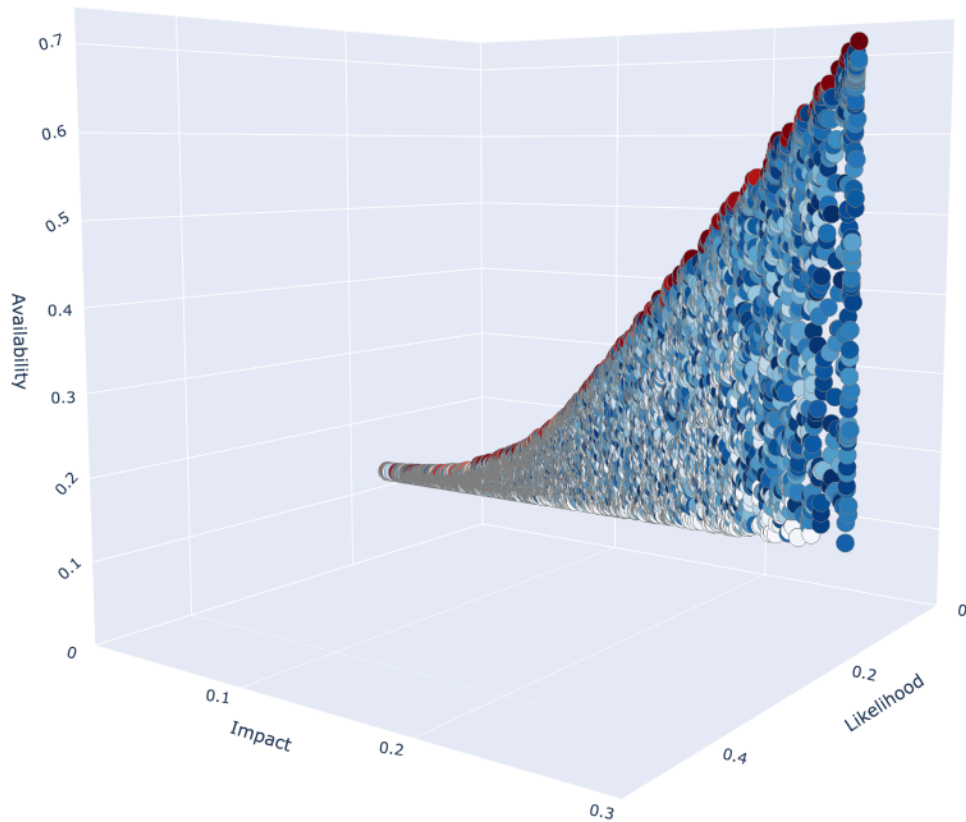


Figure 6: Pareto fronts derived over 10,000 optimisation trials in the BlackEnergy case study. Countermeasure portfolios were optimised to minimise both the likelihood of a successful attack and the probability of severe impact in CPS, while maximising CPS availability.

severe impact even when individual node exposure is significantly reduced.

Lastly, we conducted a frequency-based heuristic analysis of Pareto-optimal portfolios across multiple optimisation runs to identify and recommend countermeasures that best mitigate the BlackEnergy attack. As shown in Figure 7, vulnerabilities V1 through V7 exhibit relatively similar bar heights, indicating that mitigation must adopt a distributed strategy across multiple vulnerability nodes concurrently.

Such a strategy inherently demands greater resource investment and operational effort. In contrast, applying mitigations only to a limited subset of the countermeasure portfolio, such as V1 and V2, delivers only partial effectiveness. In this scenario, if just two of the seven top-ranked mitigations are implemented,

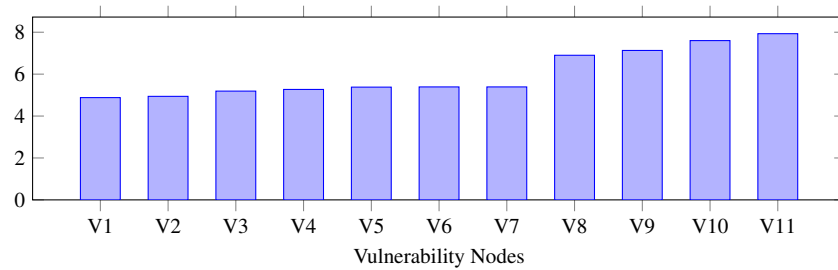


Figure 7: Average rank positions of mitigation probabilities across 100 runs of 10,000 optimisation trials in each run. Nodes are ranked based on the relative magnitude of their mitigation probabilities in the optimal portfolios, with rank 1 indicating the highest mitigative effectiveness.

the estimated mitigation effectiveness is approximately $2/7 \times 100 = 28.57\%$ of that should the full portfolio be implemented. This highlights the limitation of narrow mitigation strategies, which risk leaving critical attack paths unaddressed.

In summary, the key findings from the framework’s application to the Ukrainian power grid attack are:

- Increasingly linear relationship between impact probability and system availability at higher impact probability levels.
- Pareto fronts appear clustered near a similar value along the attack likelihood axis, suggesting limited variation in attack likelihood across optimisation trials.
- Aggressive mitigation improves availability, but does not fully suppress the residual risk of severe impact on the CI.
- Mitigation must adopt a distributed strategy across multiple vulnerability nodes concurrently.

These insights equip CI practitioners with the rationale to adopt a multi-pronged mitigation strategy tailored to the dynamics of BlackEnergy-like threats. Firstly, CI practitioners should invest in early-stage interventions to reduce exposure before the system enters high-risk zones. Secondly, the clustering of Pareto fronts around similar attack likelihood values calls for prioritising interventions based on impact severity and system availability, rather than likelihood alone. Even when near-total mitigation coverage is pursued aggressively, residual risks may persist. This warrants the need to complement countermeasure portfolios with real-time

anomaly detection, automated containment mechanisms, or fail-safe protocols to arrest cascading failures. Finally, CI practitioners should adopt mitigation strategies designed to target multiple vulnerabilities in parallel to enhance CI resilience.

4.2. Railway CBTC System Attack

Next, we shift our focus to a cyber-physical attack scenario involving a railway CBTC system. To construct a plausible threat model, we draw upon the first author’s years of expertise and domain-specific knowledge of railway CBTC systems, complemented by insights from literature that discuss CBTC architecture, vulnerabilities, and risk assessment methods. Synthesising these insights, we formulate a hypothetical cyber-physical attack path that targets CBTC assets through a chain of associated cyber-physical vulnerabilities. These relationships are instantiated within a Bayesian Network model, as illustrated in Figure 8.

As the attack scenario is hypothetical, the vulnerabilities in this case study are not linked to any known CVE entries. To address this limitation, CVSS 3.1 vectors were constructed by referencing *analogous vulnerabilities* catalogued in the NVD, which bear semantic and structural alignment with the hypothetical vulnerabilities. Initial exposure probability estimates were heuristically derived using Equation 3, and subsequently refined using the Bayesian latent variable approach outlined in Equation 5.

To validate the robustness of these estimates, we perform a comparative analysis against an EPSS-based prior. Although EPSS scores are natively unavailable for non-CVE vulnerabilities, this comparison serves as a sensitivity check to determine if the exposure probabilities remain consistent when calibrated against empirical exploitation trends. By contrasting the CVSS-based estimates with a synthetic EPSS-based prior, we can assess whether the risk assessment remains stable across different probabilistic assumptions regarding the threat landscape.

Table 7: Comparison of Joint Conditional Probabilities for Exposure and Impact of H3_Disrupt_Train_Operation Based on CVSS and EPSS Prior Distributions

State	CVSS-Based		EPSS-Based	
	ϕ_{Exposure}	ϕ_{Impact}	ϕ_{Exposure}	ϕ_{Impact}
(0)	0.1256	1.0000	0.1254	1.0000
(1)	0.8744	0.0000	0.8746	0.0000

Table 7 presents a side-by-side comparison of the conditional probability distributions for exposure and impact associated with the primary attacker goal:

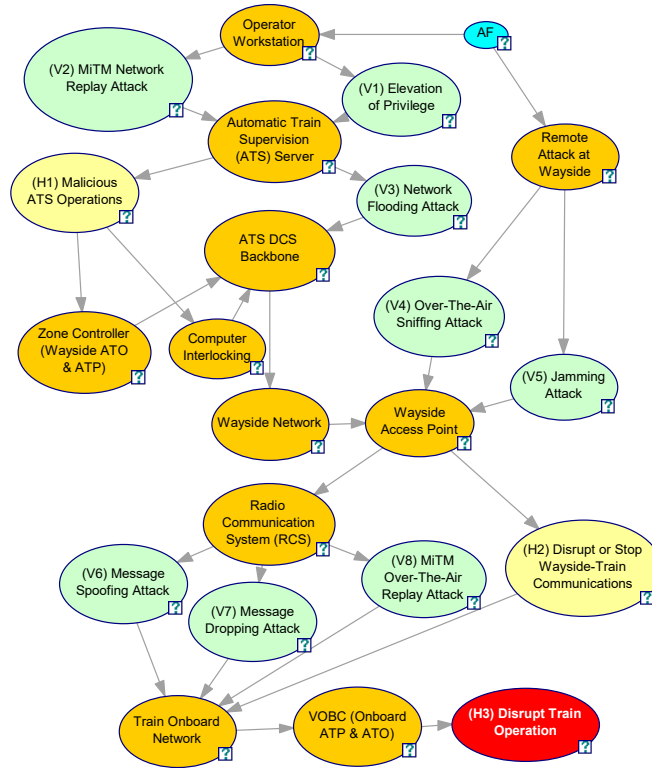


Figure 8: Bayesian Network of a hypothetical cyber-physical attack on a railway CBTC system. Node colours denote assets (orange), vulnerabilities (green), hazards (yellow), attack feasibility (cyan), and attacker goal (red). The graph shows how vulnerability and attack techniques cascade to CBTC subsystems, supporting probabilistic risk assessment. A high-resolution version is available in the project’s GitHub repository ([18]).

H3_Disrupt_Train_Operation. The CVSS-based results indicate a posterior probability of attack success of $P(E) = 0.1256$ (using an AF modifier of $\phi = 1.0$) and a conditional probability of severe impact of $P(I) = 1.0000$, yielding a risk score of $R = P(E) \times P(I) = 12.56\%$. Although this score is relatively low, the analysis reveals absolute certainty of a critical system impact if the attack path is realised. This findings highlights a significant vulnerability within the system architecture. While the likelihood of exploitation is limited, the lack of resilience against a successful breach ensures a catastrophic outcome. Consequently, the results suggest that preventive strategies must be prioritised to reduce the probability of entry, as the current system configuration offers no mitigation for the impact itself once the goal is achieved.

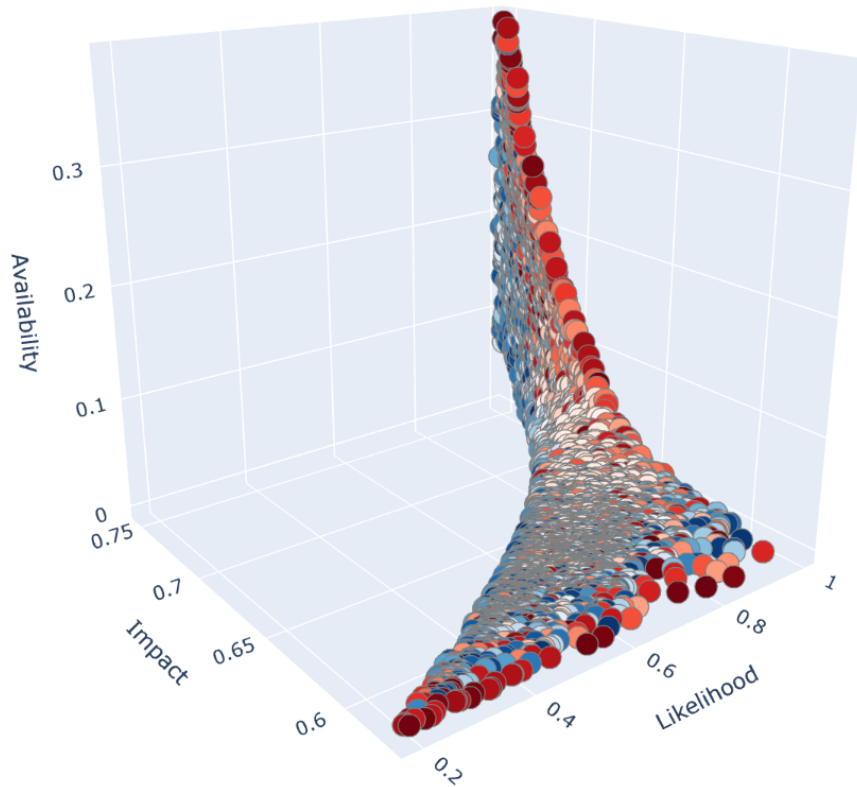


Figure 9: Pareto fronts derived over 10,000 multi-objective optimisation trials in the railway CBTC case study

Next, we conducted optimisation experiments, separately using calibrated CVSS-based priors and EPSS-based priors to evaluate differences in outcomes. In both cases, the derivation of the Pareto fronts (Figure 9) illustrates a trade-off between exposure, impact, and availability. The results reveal a consistent relationship where the likelihood of severe impact remains elevated across all levels of attack success. Dense solution clusters are observed near $Likelihood \approx 1$, indicating strong model confidence that attacks are likely to succeed under most mitigation configurations. Furthermore, the analysis demonstrates that the probability of severe impact remains significant, typically ranging between 0.55 and 0.75. This suggests that the optimisation process prioritises incremental improvements to maximise system availability, which remains constrained within the 0 to 0.4 range, rather than seeking to prevent compromise or fully suppress the resulting impact altogether.

Table 8: Comparison of top-performing countermeasure portfolios from the railway CBTC case study using calibrated CVSS-based and EPSS-based priors

Metric	CVSS-based (Trial 8361)	EPSS-based (Trial 9234)
Countermeasure portfolio	V1:0.9986, V2:0.9883, V3:0.9788, V4:0.9994, V5:0.9929, V6:0.9961, V7:0.9579, V8:0.9914	V1:0.9759, V2:0.9778, V3:0.9792, V4:0.9835, V5:0.9942, V6:0.9873, V7:0.9862, V8:0.9532
Probability of severe impact	0.7581	0.7559
Availability	0.4694	0.4462
Total execution time	0h 4m 31s	0h 4m 23s

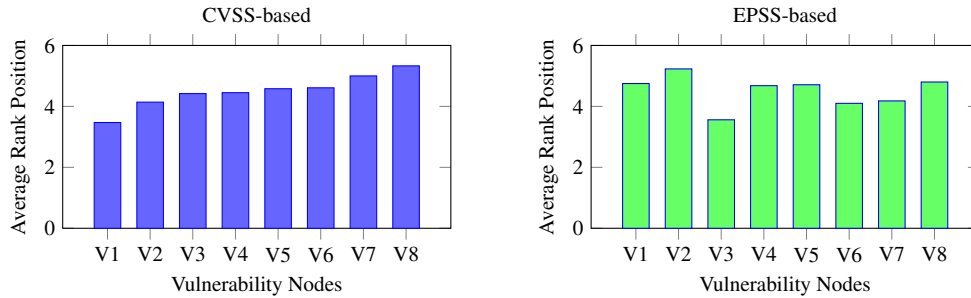


Figure 10: Side-by-side comparison of average mitigation rank positions across 100 optimisation runs (10,000 trials each) using calibrated CVSS-based and EPSS-based priors. Lower values indicate higher mitigative effectiveness.

The top-performing countermeasure portfolios are presented in Table 8. The solutions reflect a broad system-wide defence strategy in the scenario of a railway CBTC attack, with near-maximal mitigation across all variables. Although the calibrated CVSS-based solution achieves marginally higher availability (0.4694 vs. 0.4462), the EPSS-based trial exhibits a slightly lower probability of severe impact (0.7559 vs. 0.7581).

Lastly, we analysed Pareto-optimal portfolios obtained from repeated optimisation runs using both calibrated CVSS-based and EPSS-based priors, applying a frequency-based ranking to identify which vulnerability nodes were most consistently selected for Pareto-optimal countermeasure portfolios. There were visible differences between results derived from calibrated CVSS-based and EPSS-based priors respectively. As illustrated in Figure 10, the calibrated CVSS-based distribution exhibits a largely uniform pattern, with V1 exhibiting the strongest mitigation effect. In contrast, the EPSS-based distribution is more varied, with V3, V6, and V7 exhibiting higher mitigation effects relative to other nodes.

In summary, the key findings from the framework’s application to the railway CBTC system attack are:

- No marked differences between optimisation results based on EPSS and CVSS priors, respectively.
- Optimisation results favour system availability over attack prevention.
- Countermeasure portfolios show near-maximal mitigation across all vulnerabilities, reflecting a system-wide defence approach.
- Frequency analysis shows uniform emphasis in countermeasure portfolios derived from calibrated CVSS-based priors, while portfolios derived from EPSS-based priors indicate more targeted mitigation strategies.

4.3. Trade-offs and Practitioner Guidance

In interpreting the results of our three case studies, it is important to distinguish scenario-specific behaviours from properties of the framework itself. Patterns such as the shapes of Pareto fronts, the prominence of specific vulnerabilities, or clustering effects in the BlackEnergy and CBTC experiments stem from the particular architectures, threat models, and parameter settings of those scenarios. In contrast, the ability to generate Pareto-optimal countermeasure portfolios, quantify trade-offs between exposure, impact, and availability, and rank mitigation options via frequency-based heuristics are general characteristics of our proposed method that should extend to a broad range of CI deployments.

These findings provide practical guidance for CI practitioners regarding the navigation of security trade-offs. The results indicate that complementary vulnerability scoring metrics such as CVSS, EPSS, LEV, and KEV can be used flexibly even when vulnerabilities lack CVE identifiers. Specifically, the integration of LEV and KEV metrics ensures that confirmed exploitation evidence and local environmental factors take precedence in the prioritisation process. This multidimensional approach, supported by frequency analysis for the comparative evaluation of results, enables more targeted mitigation strategies under tight resource and real-time constraints.

A central insight from our evaluation is that incident mitigation in CI inherently involves a three-way trade-off between exposure, impact, and system availability. Across all case studies, the optimisation results reveal regions where reducing the likelihood of successful attack or severe impact begins to incur disproportionately high availability costs, as well as regions where additional mitigation

yields diminishing returns in risk reduction. In practice, operators must therefore balance tolerable residual exposure and impact against the need to keep CI services online, rather than pursuing maximal mitigation in isolation.

5. Discussion and Future Work

Framework Applicability to Real-World Attacks. All three case studies, including the solar PV inverter running example in Section 3, demonstrate the applicability and utility of our proposed framework in supporting real-time, adaptive decision-making needs for real-world attacks. As new information becomes available, elements such as CPS assets, probabilistic estimates of attack likelihood, impact severity, system availability, and candidate countermeasure profiles, comprising mitigation probabilities, are continuously updated via a feedback loop driven by real-time monitoring and computationally efficient multi-objective optimisation.

From a deployment perspective, the framework presupposes access to architectural knowledge, vulnerability metadata such as CVEs, and attack telemetry to update evidence in the BN. It is designed to integrate as an analytical back-end that can be invoked from existing Security Operations Centre (SOC) workflows. In particular, the framework can serve as a complementary decision-support service that consumes alerts and configuration data, rather than replacing existing SOC tooling. Our experiments in this work demonstrate that multi-objective optimisation can be parallelised to ensure runtimes compatible with operational timeframes. However, practical deployments will require engineering trade-offs between model granularity, update frequency, and available compute resources to ensure acceptable overhead in real-time or near-real-time settings.

Repeatability of Optimisation Outcomes. An important consideration arising from our research concerns the repeatability of outcomes, such as countermeasure portfolios, produced by multi-objective optimisation trials in response to identical model configurations and threat information. This directly relates to the stability and variance of Pareto fronts across repeated optimisation runs. To evaluate this, we pose the question: *What configuration of trial count is sufficient to ensure that the resulting Pareto front remains relatively consistent across independent multi-objective optimisation runs?*

To address this research question, we evaluated the nearness and clustering behaviour of Pareto fronts generated from 100, 1000, 5000, and 10,000 trials, each repeated over 100 optimisation runs. Comparison of the Pareto fronts across experimental configurations reveals that lower trial counts (e.g. 100) result in considerable dispersion and variability across runs, whereas higher trial counts (e.g.

5000 and 10,000) yield denser, more structurally consistent front distributions across objective space.

To derive a quantitative measure and comparison of cluster density, Kernel Density Estimation (KDE) [7] was employed, following a validation of unimodality of the distributions of attack likelihood, impact probability, and availability. The KDE-derived density metrics are summarised in Table 9. Taken together, these findings support the conclusion that a configuration of at least 5,000 trials is sufficient to generate consistent and structurally reliable Pareto fronts across independent multi-objective optimisation runs. However, for applications demanding finer resolution or more robust density differentiation, such as real-time countermeasure ranking or adaptive planning, a 10,000-trial configuration may offer marginally improved fidelity, albeit at the expense of execution time.

Table 9: Comparison of KDE-derived density metrics for Pareto-optimal solutions across trial configurations (100 runs each)

Metric	100 trials	1,000 trials	5,000 trials	10,000 trials
Average KDE	601.17	543.70	359.65	395.99
Minimum density	136.64	51.13	31.01	45.91
Maximum density	1130.66	1041.85	698.14	887.52
Density variance	62,435.93	84,427.79	36,824.83	56,210.58
Density entropy	4.51	4.44	4.43	4.40

Concurrency and Computational Efficiency. The optimisation experiments conducted in this research underscore the critical role of concurrency in enhancing computational efficiency and responsiveness for multi-objective decision-making in CI. Using the Python `concurrent.futures` module, we achieved substantial reductions in cumulative optimisation time (Table 10).

Table 10: Comparison of execution times for 3 runs of 10,000 trials each

Configuration	Optuna	Optuna + <code>concurrent.futures</code>
Total execution time	15 mins 3 secs	5 mins 10 secs

Future Work. To further strengthen real-time decision-making capabilities in CI environments, future work should explore several complementary directions that address the key challenges identified in our research.

First, our research highlighted the promise of frequency-based heuristics as a supplementary analytical layer beyond individual optimisation outcomes. However, their empirical nature prompts a critical question: *To what extent can such heuristically derived recommendations be relied upon in real-time, safety-critical CI environments?* Addressing this question presents a valuable avenue for future work, particularly through comparative evaluation with empirical data. Future work could also extend optimisation to explicitly account for resilience alongside system availability.

Second, the stability of Pareto fronts across repeated optimisation trials remains central to ensuring decision robustness. Low trial counts were shown to produce high variance in outcomes, which may undermine the trustworthiness of mitigation recommendations. Future investigations should therefore develop convergence diagnostics to establish sufficiency thresholds for trial configurations, and to measure the robustness of optimisation solutions.

Third, the incorporation of hybrid confidence-calibrated exposure probability assessments presents a promising direction for performing vulnerability assessment in practical deployments. Such hybrid approaches are particularly relevant in guiding real-world incident mitigation strategies that must adapt in real time to evolving attacks and dynamic threat intelligence. Furthermore, the approach is inherently extensible, facilitating the integration of diverse vulnerability scoring systems such as CVSS, EPSS, LEV, and KEV to refine the quantification of exposure estimates. Future work could further leverage this multidimensional approach to refine decision support, enabling a more comprehensive and data-informed basis for prioritising countermeasures as new threat intelligence becomes available.

Finally, architectural improvements and mechanisms could be explored to dynamically rebalance the factors employed in impact calculations (as outlined in Section 3.3), thereby enabling the generation of countermeasure portfolios that reflect evolving runtime priorities. This may include structural enhancements such as the incorporation of noisy-OR gates to improve agility in assimilating new evidence, and to better support adaptive decision-making.

Collectively, these directions aim to further improve a real-time, adaptive decision support framework for mitigating cyber incidents in CI.

6. Related Work

Probabilistic Modelling in Cybersecurity. BNs are highly effective in synthesising heterogeneous data for cybersecurity modelling, particularly when historical

attack data is sparse [8, 20]. Prior studies [44, 34, 42, 23] underscore their utility in dynamic decision-making. Bhosale et al. [5, 6] further integrated hazard, vulnerability, and asset connectivity into Bayesian Belief Networks (BBNs) using AutomationML for real-time data exchange. However, existing frameworks often overlook the operational trade-offs of security interventions, such as asset degradation or failure from software patching, and do not account for legacy system constraints and resource limitations. Furthermore, a heavy reliance on CVSS v3.1 scores limits adaptability to shifting threat landscapes where probabilistic insights from EPSS [21] are required. Our research addresses these gaps by proposing a consequence-aware, iterative framework that couples confidence-calibrated exposure probability with adaptive decision-support.

Consequence-Driven Security Assessment. Beyond modelling attack propagation, effective CI decision-making must account for the consequences of cyber-physical incidents. Kim et al. [24] incorporate a consequence layer within BN models to quantify impact propagation in exploited ICSs, detailing functional interdependencies and infrastructure-wide effects. ACTISM [19] similarly adopts a consequence-driven approach for dynamic, iterative security modelling in automotive systems. In parallel, Amro et al. [3] propose a consequence-driven framework rooted in FMECA that aligns well with CI environments. Although these approaches support iterative assessment, their transformation into adaptive tools hinges on modelling realistic, multi-stage attacks. Our research integrates system-level functional dependencies into BN structures informed by empirical failure modes, explicitly modelling uncertainty within exposure computations to enable responsive decision-making.

Decision Support for CI Incidents. Research has explored diverse methodologies for real-time CPS decision-making under uncertainty. Zaman et al. [47] propose a Markov Decision Process (MDP) framework for optimising responses to hazards such as fire and power outages. Javornik et al. [22] introduce a mission-centric DSS to guide cybersecurity experts in selecting resilient IT configurations. While providing structured resilience assessments, these frameworks often lack specific focus on the adversarial tactics and non-linear cascading risks inherent in CI incidents. To address these limitations, our research employs BN structures where nodes represent CPS assets, vulnerabilities, and hazards. This approach facilitates dynamic modelling of risk propagation and supports adaptive decision-making that reflects evolving threat scenarios and system complexity.

Multi-Objective Optimisation. Decision-making in CI incident response must balance cybersecurity, safety, and operational resilience. Rehak et al. [35] introduce a methodology for assessing CI resilience by evaluating robustness, recovery, and adaptive capacity. However, their model is essentially static and focused on pre-incident conditions rather than real-time response. Li et al. [29] propose a multi-objective optimisation framework for intrusion response in ICSs, prioritising Pareto-optimal strategies, yet it does not account for unknown vulnerabilities or emerging vectors. Similarly, Zebrowski et al. [48] use BNs to assess cascading impacts but assume static configurations. While Shimizu et al. [38] proposed a vulnerability management chaining framework integrating CVSS, EPSS, and KEV metrics, their work is tailored to enterprise IT and lacks the multi-objective weighting necessary to balance the high-availability requirements of CI environments. Our research addresses these limitations by using a Bayesian confidence calibration technique to model emerging threat uncertainty and implementing an iterative multi-objective optimisation cycle to tailor strategies for real-time CI incident mitigation.

Railway CBTC Systems. Several studies have examined the security of railway signalling, with varying emphasis on CBTC technologies. Xu et al. [45] present a simulation platform grounded in real-world CBTC characteristics, while Yu et al. [46] offer a comprehensive review of the architecture, cybersecurity threats, and protection strategies specific to these systems. In contrast, other research focuses on broader or legacy signalling components. For instance, Schlehuber et al. [37] examine interlocking systems without addressing CBTC explicitly, and Unger et al. [41] survey railway attack scenarios and countermeasure maturity across the sector more generally. Regarding systemic vulnerabilities, research has highlighted the risks inherent in the transition to wireless-based control. Farooq et al. [15] analyse over-the-air communications in CBTC, identifying interference susceptibility in Wi-Fi-based implementations. Oliveira et al. [33] expand on this by using Failure Mode and Effects Analysis (FMEA) to uncover risks such as message spoofing and Man-in-the-Middle (MitM) attacks that compromise communication integrity. Similarly, Soderi et al. [39] outline wireless attack scenarios with demonstrated impacts on railway safety. These findings directly inform the adversarial modelling applied in our CBTC case study, ensuring the evaluation reflects the unique cyber-physical risks inherent in modern automated rail operations.

7. Conclusion

This paper presented a real-time, adaptive decision support framework designed to help practitioners mitigate cyber-physical incidents within CI environments. The development of such a system is increasingly vital as CPSs become more deeply integrated into CIs while facing a rapidly diversifying threat landscape. A primary contribution of this work is the application of BN models to represent complex attack scenarios, enriched with system-specific and vulnerability metadata. By encoding these models in a DSL format, the framework achieves the computational efficiency required for operational time-frames, allowing for dynamic updates that support adaptive decision-making as an incident unfolds.

The framework further introduces a novel decision-support methodology for countermeasure selection based on multi-objective optimisation and frequency-based heuristic analysis. By treating mitigation probabilities as parameters within a structured search space, the system generates Pareto-optimal portfolios that balance the critical requirements of security, safety, and operational resilience. The use of frequency-based heuristics across multiple optimisation runs provides a practical bridge between complex model outputs and actionable guidance, enabling operators to identify the most robust and consistent mitigation strategies under severe resource constraints.

To address the inherent uncertainty of cyber-physical vulnerabilities, the framework incorporates a hybrid exposure probability estimation technique. This method integrates complementary vulnerability scoring metrics through a Bayesian confidence calibration process, yielding robust exposure recommendations even when faced with the incomplete or heterogeneous metadata typical of legacy CI assets.

The practical utility of this applied research was validated through evaluation across three representative scenarios: the 2015 Ukrainian power grid (BlackEnergy) attack, a solar PV inverter system and a railway signalling network. These case studies demonstrate the framework's versatility in handling diverse multi-path and multi-agent threats within the CI domain. Finally, to support transparency and facilitate further development by both practitioners and researchers, the models, source code and reference data have been made publicly available [18]. This open approach ensures that the findings can be replicated and extended to enhance the protection of the essential systems that underpin modern society.

CRedit authorship contribution statement

Shaofei Huang: Conceptualisation, Methodology, Software, Validation, Formal analysis, Investigation, Writing – Original Draft, Writing – Review & Editing,

Visualisation, Project administration. **Christopher M. Poskitt**: Conceptualisation, Methodology, Writing – Review & Editing, Supervision. **Lwin Khin Shar**: Conceptualisation, Methodology, Writing – Review & Editing, Supervision.

Declaration of Competing Interest

The authors declare that there are no conflicts of interest that could have influenced the conduct or outcomes of this research. Furthermore, this research did not receive any specific grant from funding agencies in the public, commercial or not-for-profit sectors.

Data Availability

The models and source code from this research, along with high-resolution versions of the paper’s figures are publicly available in the project’s GitHub repository ([18]).

References

- [1] Akiba, T., Sano, S., Yanase, T., Ohta, T., Koyama, M., 2019. Optuna: A Next-generation Hyperparameter Optimization Framework, in: Proceedings of the 25th ACM SIGKDD international conference on knowledge discovery & data mining, pp. 2623–2631. doi:10.1145/3292500.333070.
- [2] Akoglu, L., Tong, H., Koutra, D., 2015. Graph based anomaly detection and description: a survey. *Data mining and knowledge discovery* 29, 626–688. doi:10.1007/s10618-014-0365-y.
- [3] Amro, A., Gkioulos, V., Katsikas, S., 2023. Assessing Cyber Risk in Cyber-Physical Systems Using the ATT&CK Framework. *ACM Transactions on Privacy and Security* 26, 1–33. doi:10.1145/3571733.
- [4] AutomationML Association, 2025. AutomationML Editor. <https://github.com/AutomationML/AutomationMLEditor>. Accessed: 2026-02-18.
- [5] Bhosale, P., Kastner, W., Sauter, T., 2023. Integrated Safety-Security Risk Assessment for Production Systems: A Use Case Using Bayesian Belief Networks, in: 2023 IEEE 21st International Conference on Industrial Informatics (INDIN), IEEE. pp. 1–6. doi:10.1109/INDIN51400.2023.10217926.

- [6] Bhosale, P., Kastner, W., Sauter, T., 2024. AutomationML meets Bayesian Networks: A Comprehensive Safety-Security Risk Assessment in Industrial Control Systems. *IEEE Open Journal of the Industrial Electronics Society* doi:10.1109/OJIES.2024.3439388.
- [7] Chen, Y.C., 2017. A tutorial on kernel density estimation and recent advances. *Biostatistics & Epidemiology* 1, 161–187. doi:10.1080/24709360.2017.1396742.
- [8] Chockalingam, S., Pieters, W., Teixeira, A., van Gelder, P., 2017. Bayesian Network Models in Cyber Security: A Systematic Review, in: *Secure IT Systems: 22nd Nordic Conference, NordSec 2017, Tartu, Estonia, November 8–10, 2017, Proceedings 22*, Springer. pp. 105–122. doi:10.1007/978-3-319-70290-2_7.
- [9] CISA, 2026. Known Exploited Vulnerabilities Catalog. <https://www.cisa.gov/known-exploited-vulnerabilities-catalog>. Accessed: 2026-02-18.
- [10] Dabrowski, A., Ullrich, J., Weippl, E.R., 2017. Grid Shock: Coordinated Load-Changing Attacks on Power Grids: The Non-Smart Power Grid is Vulnerable to Cyber Attacks as Well, in: *Proceedings of the 33rd Annual Computer Security Applications Conference*, pp. 303–314. doi:10.1145/3134600.313463.
- [11] Dashevskiy, S., La Spina, F., Dos Santos, D., 2025. SUN:DOWN Destabilizing the grid via orchestrated exploitation of solar power systems. <https://www.forescout.com/resources/sun-down-research-report/>. Accessed: 2026-02-18.
- [12] Decision Systems Laboratory, 2023. GeNie Modeler. <https://www.bayesfusion.com/genie/>. BayesFusion, LLC. Accessed: 2026-02-18.
- [13] Dewri, R., Poolsappasit, N., Ray, I., Whitley, D., 2007. Optimal Security Hardening Using Multi-objective Optimization on Attack Tree Models of Networks, in: *Proceedings of the 14th ACM Conference on Computer and Communications Security*, pp. 204–213. doi:10.1145/1315245.1315272.

- [14] Drath, R., Luder, A., Peschke, J., Hundt, L., 2008. Automationml - the glue for seamless automation engineering, in: 2008 IEEE International Conference on Emerging Technologies and Factory Automation, IEEE. pp. 616–623. doi:10.1109/ETFA.2008.4638461.
- [15] Farooq, J., Soler, J., 2017. Radio Communication for Communications-Based Train Control (CBTC): A Tutorial and Survey. *IEEE Communications Surveys & Tutorials* 19, 1377–1402. doi:10.1109/COMST.2017.2661384.
- [16] FIRST, 2015. Common Vulnerability Scoring System v3.1: Specification Document. <https://www.first.org/cvss/v3-1/specification-document>. Accessed: 2026-02-18.
- [17] Fowler, M., 2010. *Domain-Specific Languages*. Pearson Education.
- [18] Huang, S., 2026. Bayesian and Multi-Objective Decision Support for Real-Time Cyber-Physical Incident Mitigation - Project Repository. <https://github.com/shaofeihuang/cps-bayesian-optuna-dss>. Accessed: 2026-02-18.
- [19] Huang, S., Poskitt, C.M., Shar, L.K., 2024a. ACTISM: Threat-informed Dynamic Security Modelling for Automotive Systems. arXiv preprint arXiv:2412.00416 doi:10.48550/arXiv.2412.00416.
- [20] Huang, S., Poskitt, C.M., Shar, L.K., 2024b. Security Modelling for Cyber-Physical Systems: A Systematic Literature Review. *ACM Transactions on Cyber-Physical Systems* doi:10.1145/3776549.
- [21] Jacobs, J., Romanosky, S., Edwards, B., Adjerid, I., Roytman, M., 2021. Exploit Prediction Scoring System (EPSS). *Digital Threats: Research and Practice* 2, 1–17. doi:10.1145/3436242.
- [22] Javorník, M., Husák, M., 2022. Mission-centric decision support in cybersecurity via Bayesian Privilege Attack Graph. *Engineering Reports* 4, e12538. doi:10.1002/eng2.12538.
- [23] Khosravi-Farmad, M., Ghaemi-Bafghi, A., 2020. Bayesian Decision Network-Based Security Risk Management Framework. *Journal of Network and Systems Management* 28, 1794–1819. doi:10.1007/s10922-020-09558-5.

- [24] Kim, A., Oh, J., Kwon, K., Lee, K., 2022. Consider the Consequences: A Risk Assessment Approach for Industrial Control Systems. *Security and Communication Networks* 2022, 3455647. doi:10.1155/2022/3455647.
- [25] Knapik, B.T., van der Vaart, A.W., van Zanten, J.H., 2011. Bayesian Inverse Problems with Gaussian Priors. *The Annals of Statistics* 39, 2626 – 2657. doi:10.1214/11-AOS920.
- [26] Kumar, A., Saini, M., Saini, D.K., Badiwal, N., 2021. Cyber physical systems-reliability modelling: critical perspective and its impact. *International Journal of System Assurance Engineering and Management* 12, 1334–1347. doi:10.1007/s13198-021-01305-6.
- [27] Kumar, R., Kela, R., Singh, S., Trujillo-Rasua, R., 2022. APT attacks on industrial control systems: A tale of three incidents. *International Journal of Critical Infrastructure Protection* 37, 100521. doi:10.1016/j.ijcip.2022.100521.
- [28] Küppers, F., Kronenberger, J., Schneider, J., Haselhoff, A., 2021. Bayesian Confidence Calibration for Epistemic Uncertainty Modelling, in: 2021 IEEE Intelligent Vehicles Symposium (IV), IEEE. pp. 466–472. doi:10.1109/IV48863.2021.9575841.
- [29] Li, X., Zhou, C., Tian, Y.C., Qin, Y., 2018. A Dynamic Decision-Making Approach for Intrusion Response in Industrial Control Systems. *IEEE Transactions on Industrial Informatics* 15, 2544–2554. doi:10.1109/TII.2018.2866445.
- [30] Mell, P., Scarfone, K., Romanosky, S., 2007. Common Vulnerability Scoring System. *IEEE Security & Privacy* 4, 85–89. doi:10.1109/MSP.2006.145.
- [31] Mell, P., Spring, J., 2025. Likely Exploited Vulnerabilities - A Proposed Metric for Vulnerability Exploitation Probability. NIST CSWP 41 doi:10.6028/NIST.CSWP.41.
- [32] NIST, 2025. National Vulnerability Database. <https://nvd.nist.gov/>. Accessed: 2026-02-18.
- [33] Oliveira, J., Carvalho, G., Cabral, B., Bernardino, J., 2020. Failure Mode and Effect Analysis for Cyber-Physical Systems. *Future Internet* 12, 205. doi:10.3390/fi12110205.

- [34] Poolsappasit, N., Dewri, R., Ray, I., 2011. Dynamic Security Risk Management Using Bayesian Attack Graphs. *IEEE Transactions on Dependable and Secure Computing* 9, 61–74. doi:10.1109/TDSC.2011.34.
- [35] Rehak, D., Senovsky, P., Hromada, M., Lovecek, T., 2019. Complex approach to assessing resilience of critical infrastructure elements. *International journal of critical infrastructure protection* 25, 125–138. doi:10.1016/j.ijcip.2019.03.003.
- [36] SANS, 2016. Analysis of the cyber attack on the Ukrainian power grid. *Electricity Information Sharing and Analysis Center (E-ISAC)* 388, 3.
- [37] Schlehuber, C., Heinrich, M., Vateva-Gurova, T., Katzenbeisser, S., Suri, N., 2017. A Security Architecture for Railway Signalling, in: *Computer Safety, Reliability, and Security: 36th International Conference, SAFECOMP 2017, Trento, Italy, September 13-15, 2017, Proceedings* 36, Springer. pp. 320–328. doi:10.1007/978-3-319-66266-4_21.
- [38] Shimizu, N., Hashimoto, M., 2025. Vulnerability Management Chaining: An Integrated Framework for Efficient Cybersecurity Risk Prioritization. arXiv preprint arXiv:2506.01220 .
- [39] Soderi, S., Masti, D., Hämäläinen, M., Iinatti, J., 2023. Cybersecurity Considerations for Communication Based Train Control. *IEEE Access* 11, 92312–92321. doi:10.1109/ACCESS.2023.3309005.
- [40] Taylor, J.M., Sharif, H.R., 2017. Security challenges and methods for protecting critical infrastructure cyber-physical systems, in: *2017 International Conference on Selected Topics in Mobile and Wireless Networking (MoWNeT)*, pp. 1–6. doi:10.1109/MoWNet.2017.8045959.
- [41] Unger, S., Heinrich, M., Scheuermann, D., Katzenbeisser, S., Schubert, M., Hagemann, L., Iffländer, L., 2023. Securing the Future Railway System: Technology Forecast, Security Measures, and Research Demands. *Vehicles* 5, 1254–1274. doi:10.3390/vehicles5040069.
- [42] Wang, L., Jajodia, S., Singhal, A., Frigault, M., Wang, L., Jajodia, S., Singhal, A., 2017. Measuring the overall network security by combining CVSS scores based on attack graphs and Bayesian networks. *Network Security Metrics* , 1–23doi:10.1007/978-3-319-66505-4_1.

- [43] Wunder, J., Kurtz, A., Eichenmüller, C., Gassmann, F., Benenson, Z., 2024. Shedding Light on CVSS Scoring Inconsistencies: A User-Centric Study on Evaluating Widespread Security Vulnerabilities, in: 2024 IEEE Symposium on Security and Privacy (SP), IEEE. pp. 1102–1121. doi:10.1109/SP54263.2024.00058.
- [44] Xie, P., Li, J.H., Ou, X., Liu, P., Levy, R., 2010. Using bayesian networks for cyber security analysis, in: 2010 IEEE/IFIP international conference on dependable systems & networks (DSN), IEEE. pp. 211–220. doi:10.1109/DSN.2010.5544924.
- [45] Xu, J., Chen, L., Gao, W., Zhao, M., et al., 2015. CBTC Simulation Platform Design and Study. *Journal of Computer and Communications* 3, 61. doi:10.4236/jcc.2015.39007.
- [46] Yu, Z., Wang, H., Chen, F., 2023. Security of railway control systems: A survey, research issues and challenges. *High-speed Railway* 1, 6–17. doi:10.1016/j.hspr.2022.12.001.
- [47] Zaman, M., Eini, R., Zohrabi, N., Abdelwahed, S., 2022. A Decision Support System for Cyber Physical Systems under Disruptive Events: Smart Building Application, in: 2022 IEEE International Smart Cities Conference (ISC2), pp. 1–7. doi:10.1109/ISC255366.2022.9922493.
- [48] Żebrowski, P., Couce-Vieira, A., Mancuso, A., 2022. A Bayesian Framework for the Analysis and Optimal Mitigation of Cyber Threats to Cyber-Physical Systems. *Risk Analysis* 42, 2275–2290. doi:10.1111/risa.13900.
- [49] Zhang, N.L., Poole, D., 1996. Exploiting Causal Independence in Bayesian Network Inference. *Journal of Artificial Intelligence Research* 5, 301–328. doi:10.1613/jair.305.